(1969).
[41]M. Pomerantz, Phys. Rev. **139**, A501 (1965).
[42]Rosemont Engineering, 4900 West 78th St., Minneapolis, Minn. 55424.
[43]Coherent Optics, Inc., 320 North Washington St., Rochester, N. Y. 14625.
[44]ITT, 3505 Hartley Ave., Easton, Pa. 18043.
[45]Canberra Industries, 45 Gracy Ave., Meridan, Conn. 06450.
[46]Honeywell, Inc., 1100 Virginia Dr., Fort Washington, Pa. 19034.
[47]P. E. Schoen, Ph.D. thesis (The Johns Hopkins University, 1971) (unpublished).
[48]Isomet Corp., 433 Commercial Ave., Palisades Park, N. J. 07650.
[49]J. W. Cooley and J. W. Tukey, Math. Comput. **19**, 297 (1965). For an excellent review of FFT and digital FFT algorithms, see, IEEE Trans. Audio Electroacoust. AU-15 (1967).
[50]One of us (R.L.R.) is indebted to M. Karweit for his helpful assistance in implementing the FFT package.
[51]See, R. V. Churchill, *Operational Mathematics* (McGraw-Hill, New York, 1958).
[52]V. G. Cooper, Appl. Opt. **10**, 525 (1971).
[53]A. F. Jones and D. L. Misell, J. Phys. A **3**, 462 (1970).
[54]D. W. Marquandt, R. A. Bennett, and E. J. Burrell, J. Mol. Spectrosc. 7, 269 (1961); D. W. Marquandt, J. Soc. Ind. Appl. Math. B 11, 431 (1963); Chem. Eng. Prog. **55**, 65 (1959).
[55]R. Blinc, J. Stepisnik, M. Jamsek-Vilfan, and S. Zumer, J. Chem. Phys. **54**, 187 (1971).
[56]J. R. Sliker and S. R. Burlage, J. Appl. Phys. **34**, 1837 (1963); R. J. Mayer and J. L. Bjorkstam, J. Phys. Chem. Solids **23**, 619 (1962); R. M. Hill and S. K. Ichiki, Phys. Rev. **132**, 1603 (1963); Phys. Rev. **130**, 150 (1963).
[57]C. M. Wilson and H. Z. Cummins, in Ref. 25(b), p. 420
[58]Analysis of the Brillouin scattering intensity in terms of a temperature dependent p_{66}^{E} has recently been applied to rubidium dihydrogen phosphate by G. Hauret, L. Taurel, and J. P. Chapelle [Solid State Commun. **10**, 727 (1972)].
[59]Closely related formulations of the scattering problem for linearly coupled modes in terms of Green's functions have been discussed by J. Ruvalds and A. Zawadowski and by E. F. Steigmeier, G. Harbeke, and R. K. Wehner in Ref. 25(b), pp. 29 and 396. Ruvalds and Zawadowski have explicitly considered the piezoelectric coupling of acoustic modes to overdamped soft modes, and their Eqs. (9) are of the same form as our susceptibilities in Table II.

PHYSICAL REVIEW B VOLUME 7, NUMBER 9 1 MAY 1973

Light Scattering by Phonons and Magnons in $NaNiF_3$

R. V. Pisarev,* P. Moch, and C. Dugautier
Laboratoire de Physique des Solides, Associé au Centre National de la Recherche Scientifique, Université de Paris VI, E. N. S., 24, Rue Lhomond, Paris V, France
(Received 24 October 1972)

The weak four-sublattice ferromagnet $NaNiF_3$ shows one- and two-magnon Raman scattering. The two-magnon scattering is perfectly described by a two-sublattice isotropic cubic antiferromagnet model with one exchange integral between magnetic neighbors ($J = 41.8$ cm^{-1}). The two one-magnon low-frequency lines, centered at 6.5 and 11.5_5 cm^{-1} have been studied as a function of the direction and the amplitude of an applied magnetic field and versus the temperature. A two-sublattice model, taking into account the isotropic exchange, the antisymmetric and symmetric anisotropic exchanges, and the single-ion anisotropy, provides a satisfactory agreement with the experiment. The most important term after the isotropic exchange is the Dzyaloshinski–Moriya antisymmetric exchange, but other coefficients are necessary to give an account of the observed properties: Seven of them were derived from our experimental data, which enables us to explain all the known magnetic properties of $NaNiF_3$. Besides this we discuss the one-phonon Raman scattering of $NaNiF_3$.

I. INTRODUCTION

Below $T_N \simeq 150$ °K, $NaNiF_3$ is a weak ferromagnet.[1] In the paramagnetic phase it crystallizes in the orthorhombic system, its most probable space group being D_{2h}^{16} (Ref. 2): Such a structure is obtained by deformation of the usual cubic perovskite arrangement, the orthorhombic axes a, b, and c being, respectively, parallel to the $\langle 110\rangle$, $\langle 1\bar{1}0\rangle$, and $\langle 001\rangle$ directions related to the pseudoregular octahedron (Fig. 1). There are four magnetic ions per unit cell, and below T_N the magnetic structure is of $G_aC_bF_c$ type; however, practically, it can be considered as a two-magnetic-sublattice weakly canted ferromagnet[3] (G_aF_c): This approximation is certainly sufficient, at least as long as one studies low-frequency excitations only; it leads to two magnon branches, one of which has been observed at $\vec{k} = \vec{0}$ by antiferromagnetic resonance.[4] A spin-flip transition can be obtained, using a rather moderate field (~20 kG) along the a axis[4]: The direction of each sublattice magnetization becomes nearly parallel to c instead of a, with a canting along a instead of c.

Our principal motivations for studying Raman scattering in $NaNiF_3$ were the following: (i) to investigate the two-magnon Raman scattering in order to test the adequacy of the two-sublattice isotropic antiferromagnet model near the Brillouin-zone boundaries, and to derive a precise value of the exchange integral; (ii) to study the two low-frequency magnon branches at $\vec{k} = \vec{0}$ with an applied

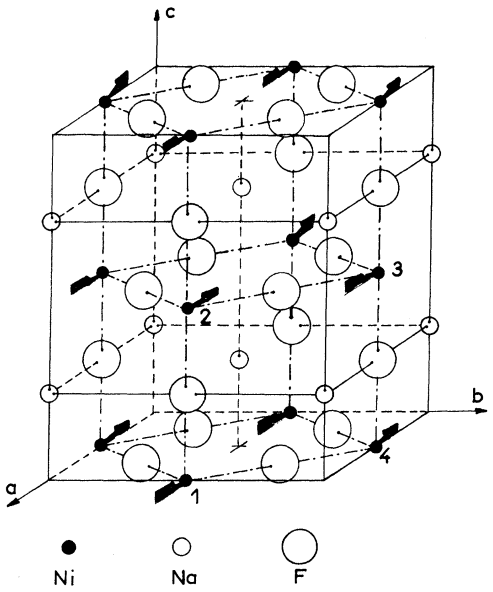

FIG. 1. Unit cell of $NaNiF_3$.

magnetic field, and then get better information about the different parameters responsible for the anisotropy; (iii) finally, we found it interesting to study the phonon scattering, which is forbidden for the cubic perovskite structure, but allowed for D_{2h}^{16}, and to compare experimental results with theoretical predictions.

II. EXPERIMENTS

The $NaNiF_3$ crystals were grown by a double decomposition technique following the reaction

$$3NaF + NiCl_2 \rightarrow NaNiF_3 + 2NaCl\,.$$

We used two samples, each with its faces perpendicular to the a, b, and c axes, which are the principal axes of the dielectric tensor; this minimizes errors due to birefringence which, for other crystal orientations, makes a correct analysis of selection rules difficult. Most of the experiments were performed with a crystal immersed in superfluid helium (2 °K), using the $\lambda = 5145$-Å line of an argon-ion laser. A magnetic field up to 50 kG was provided by a superconducting coil. The temperature dependence was also studied, using an exchange-gas cryostat, but our experimental arrangement allowed the presence of a magnetic field only at 2 °K. For low-frequency spectra, we used a single-mode laser and an iodine cell, in order to reabsorb the elastically scattered light.

III. PHONON SCATTERING

At $\vec{k} = \vec{0}$, for a D_{2h}^{16} symmetry, one expects 60 normal modes (including the three acoustical zero-frequency modes). Using a standard group-theoretical analysis, we predict 24 Raman-active vibrations, which can be classified according to the four even irreducible representations[5] of D_{2h} as follows:

$$7\Gamma_1^+(aa, bb, cc) + 5\Gamma_2^+(ac, ca) + 7\Gamma_3^+(ab, ba) + 5\Gamma_4^+(bc, cb)\,.$$

In the above expression, the allowed polarizations[6] for each irreducible representation are written between brackets. The occurrence of the Raman-active modes can be derived from the cubic O_h perovskite symmetry in the following way: They arise from the points R, M, and X of the cubic Brillouin-zone boundaries, which fall at the center of the Brillouin zone related to the D_{2h} symmetry which involves four $NaNiF_3$ groups per unit cell (Fig. 2); a calculation of the D_{2h} irreducible representations of interest arising from M, X, and R can be performed, despite some complications due to the fact that, when lowering the symmetry, the crystal group becomes nonsymmorphic. The experimental results are summarized in Table I: The 2 °K spectrum is very similar to that at 300 °K; however, the lines are sharper at low temperature (typically 2 cm^{-1} at half-maximum), and the 2 °K spectrum allows the best analysis since in some

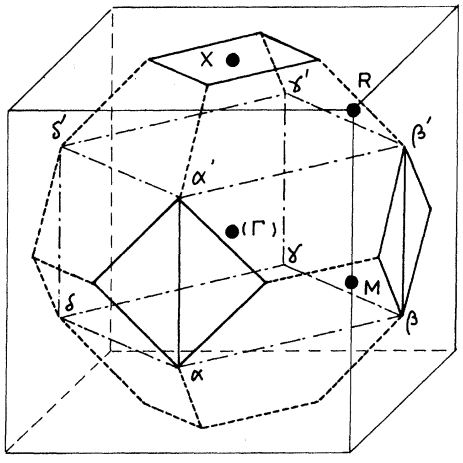

FIG. 2. Reduction of the Brillouin zone of $NaNiF_3$ due to the distortion of the cubic perovskite symmetry: (α, β, γ, δ, α', β', γ', δ') represents the Brillouin zone in D_{2h} symmetry with 4 molecules per unit cell. The large cube is the nuclear Brillouin zone in the cubic approximation: when O_h reduces to D_{2h}, M, R, and X shift to the center of the Brillouin zone. Finally, the truncated octahedron is the magnetic Brillouin zone for the bimolecular two-sublattice face-centered-cubic structure.

cases two nearly adjacent lines are not resolved on the 300 °K spectrum.

One notices that the whole set of 24 theoretically expected different modes is not observed: (a) partly because, for some modes, the intensity is probably too weak to be measurable; (b) partly because some weak lines show selection rules which correspond to two or three different irreducible representations of D_{2h}. It may occur for many lines; unfortunately, experimental limitations mainly due to birefringence prevent the observation of perfectly polarized spectra, and one can definitively assign "mixed" selection rules to a given line only if the intensities for two or more polarizations are of the same order of magnitude (in the present case, with a ratio smaller than 6). Such is the case for the 140-cm^{-1} line as shown in Table I; the other lines experimentally present some residual intensity in polarizations other than the most efficient for Raman scattering. Depending on the studied spectra, for any given line, it varies from 0.5% to 12% of the corresponding most intense spectrum, and the question of a "mixed" behavior cannot be clarified.

The conclusion is that some vibrations are very insensitive to the distortion of the cubic symmetry; they then remain practically degenerate and do not show strong Raman scattering. The most striking result is the presence of only one line above 320 cm^{-1}; in the cubic perovskite similar crystals

TABLE I. Frequencies and selection rules for one-phonon scattering in $NaNiF_3$. The underlined frequencies are also observed by infrared absorption (Ref. 9).

Frequency in cm^{-1}			Irreducible representations in agreement with
2 °K	300 °K	Intensity	selections rules
108	107	weak	Γ_1^+
140	<u>136</u>	weak	$\Gamma_2^+ + \Gamma_3^+ + \Gamma_4^+$[a]
148	143	strong	Γ_1^+
159	153	very weak	Γ_3^+
174	<u>174</u>	very weak	Γ_4^+
187	179	strong	Γ_1^+
207	<u>198</u>	weak	Γ_3^+
215	212	weak	Γ_1^+
247	<u>242</u>	very weak	Γ_3^+
253		strong	Γ_1^+
294	≥ 295	weak	Γ_2^+
301	298	strong	Γ_1^+
315	<u>312</u>	weak	Γ_3^+
369	363	weak	Γ_1^+

[a]Assignment to Γ_4^+ still doubtful.

($KNiF_3$ for instance) at $\vec{k}=\vec{0}$, there are three Γ_4^- optically infrared-active odd modes with frequencies ν_1, ν_2, and ν_3, respectively, around 130, 250, and 450 cm^{-1},[7,8] and one Γ_5^- infrared-inactive odd mode probably around 200 cm^{-1}.[9] The highest vibrational modes, related to ν_3 are then nearly unaffected by the distortions responsible for the lowering of the symmetry.

Theoretically, there are 25 infrared-active modes $9\Gamma_2^-(\vec{E}\parallel b)+7\Gamma_3^-(\vec{E}\parallel c)+9\Gamma_4^-(\vec{E}\parallel a)$. Unfortunately the only published data concern unpolarized spectra of powdered samples.[9] Similar to the Raman data, the absorption spectrum is complex for low frequencies. At high frequencies there is only one strong absorption line centered at 447 cm^{-1} ($T=300$ °K), which corresponds to the well-known ν_3 Γ_4^- mode in cubic perovskites: The modes related to ν_3 almost do not see the lowering of the symmetry. Some frequencies appear simultaneously in the infrared and in the Raman spectra. The apparent mixing of odd and even modes is, here again, probably due to the quasidegeneracy of vibrational levels weakly affected by the distortion. As expected, such a mixing only happens with modes weakly active for Raman scattering.

From Table I, it appears that $7\Gamma_1^+$, $2\Gamma_2^+$, $5\Gamma_3^+$, and $1\Gamma_4^+$ modes are clearly identified from Raman-scattering results. We think that, owing to the rather complicated crystallographic structure, a more detailed analysis would be difficult. Finally, note that the symmetry D_2^4,[10] lower than D_{2h}^{16}, has been proposed for $NaNiF_3$: It would provide an alternative explanation for the simultaneous observation of some frequencies in the infrared and Raman spectra, since D_2^4 has no center of inversion. However the crystallographic arrangement is certainly very near to D_{2h}^{16}, and the occurrence of a lower symmetry would again increase the theoretically expected number of Raman-active modes.

IV. TWO- AND FOUR-MAGNON SCATTERING

At low temperature $NaNiF_3$ shows a broad Raman line in the 400–500-cm^{-1} range (Fig. 3); its frequency, shape and temperature dependence allow its identification to the two-magnon Raman scattering.

A. Two-Magnon Raman Scattering at 2° K

Two-magnon Raman scattering from a two-sublattice antiferromagnet has been extensively studied and discussed by several authors.[11–14] For the cubic symmetry case, it is well known that one observes scattering only of Γ_3^+ character.[13,15] Chinn *et al.*[13] have calculated the shape of the spectrum, with special attention to the spin-1 case, and, for $KNiF_3$, they obtained an excellent agreement with experiment. Our experimental results show that the two-magnon scattering in $NaNiF_3$ is

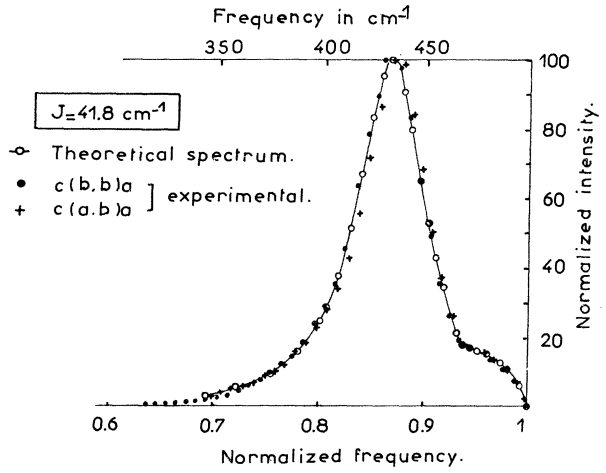

FIG. 3. Two-magnon scattering in $NaNiF_3$ at 2°K; comparison of experimental and theoretical shape (Ref. 13).

also exactly described using a cubic two-sublattice isotropic Heisenberg antiferromagnet model, with only one exchange integral between next neighbors.

(i) The shape of the spectrum does not depend on the polarization when it is observed. Moreover, the relative intensities for different polarizations can be calculated using the Γ_3^+ symmetric Raman tensor[6]:

$$\begin{pmatrix} -a_0 & 0 & 0 \\ 0 & -a_0 & 0 \\ 0 & 0 & 2a_0 \end{pmatrix} \begin{pmatrix} \sqrt{3}\,a_0 & 0 & 0 \\ 0 & -\sqrt{3}\,a_0 & 0 \\ 0 & 0 & 0 \end{pmatrix}.$$

The experimental arrangement allowed such a verification, since the a, b, and c directions are, respectively, the $\langle 110\rangle$, $\langle 1\bar{1}0\rangle$, and $\langle 001\rangle$ axes of the pseudocubic cell. If, for instance, we study the set of $c(ab)a$, $c(bb)a$, $c(bc)a$, and $c(ac)a$ spectra, we immediately conclude from the examination of the above tensor that the respective intensities have to be proportional to 100, 75, 0, and 0. Our experimental results provide the values 100, 80, 5, and 5, in excellent agreement with the theory, if we take into account the experimental uncertainties mainly due to birefringence.

(ii) The spectrum shows a maximum intensity at 438 cm^{-1}, and the cutoff frequency is 502 cm^{-1}. As shown in Fig. 3 the calculated shape fits the experimental one very well. It provides $J\langle S\rangle = 41.8 \pm 0.3$ cm^{-1} (here our convention is that for a given pair of neighboring spins i and j, the exchange is written $+J\vec{S}_i\cdot\vec{S}_j$, and not $-2J\vec{S}_i\cdot\vec{S}_j$). As shown in Sec. V, the anisotropy terms are very small compared with the isotropic exchange interactions, except for the Dzialoshinski–Moriya antisymmetric coupling. But since the spin-wave frequencies depend only on the square of this last term,[4,16] for high energies near the Brillouin-zone boundaries, the density of states essentially depends only on isotropic exchange, and consequently the two-magnon Raman scattering is very well described if we ignore anisotropy. However, for a D_{2h} symmetry and four magnetic sublattices, one can show that there are two different isotropic exchange integrals J_{12} and J_{14}, and that a rather small difference between J_{12} and J_{14} (~20%) significantly modifies the high-frequency density of states,[17] which consequently changes the shape of the two-magnon Raman scattering. We then conclude that J_{12} and J_{14} are nearly equal, and that a two-sublattice antiferromagnetic model provides a good fit with experiments. Similarly high values of next-nearest-neighbor intrasublattice exchange would strongly affect the density of states and the two-magnon Raman line shape, in contradiction with our results.

Now let us compare the two- and four-sublattice models; supposing, for simplicity, that there is an isotropic Heisenberg exchange only between first neighbors and neglecting, in a first stage, the previously mentioned anisotropy terms. Within the above approximations, if one ignores the distortions from the cubic perovskite symmetry, the two-sublattice antiferromagnet is described, using one exchange integral J, and shows a fcc arrangement of the up and down spins: The first Brillouin-zone is then a truncated octahedron. The X point in Fig. 2 is at the center of its top face. The simplest way to move from the two-sublattice to the four-sublattice antiferromagnet is by introducing two different exchange integrals J_{12} (equal to J_{34}), and J_{14} (equal to J_{23}); the Brillouin zone is then halved in such a way that the X point now lies at the center of a four-sublattice Brillouin zone, as shown on Fig. 2, which gives rise to an optical-magnon branch. More quantitatively, for the two-sublattice case, the magnon frequency is expressed by

$$\hbar\omega = zJ(1-\gamma_{\vec{k}}^2)^{1/2}. \tag{1}$$

z is the number of antiferromagnetic first neighbors ($z=6$) and $\gamma_{\vec{k}} = (1/z)\sum_j e^{i\vec{k}\cdot\vec{\delta}_j}$, where $\vec{\delta}_j$ is the position vector of the first neighbor j when the central atom is the origin. At the X point

$$\hbar\omega(X) = \sqrt{32}\,J. \tag{2}$$

For the four-sublattice case, the frequency of the optical branch at $\vec{k}=\vec{0}$ is given by the expression[17]

$$\hbar\omega = (32\,J_{12}J_{14})^{1/2}. \tag{3}$$

With such a model the acoustic branch has, indeed, a zero frequency at $\vec{k}=\vec{0}$. At this stage both branches show a twofold degeneracy. The anisotropy terms have now to be taken into account: They slightly modify the frequencies and, in the case of

the magnetic point group of $NaNiF_3$, $D_{2h}(C_{2h})$, they remove the degeneracies. J_{12} and J_{14} are expected to be of the same order of magnitude, and we are then left with two acoustical branches of low frequency and two optical branches of high frequency. A direct calculation of the irreducible representations of the excitations in C_{2h},[18] using the Loudon's method[19] shows that there are $2\Gamma_1^+$ and $2\Gamma_2^+$ magnons; the two acoustic magnons, respectively, belong to Γ_1^+ and Γ_2^+, as well as the optical ones.

In the limiting case, where J_{12} and J_{14} are equal, the expressions (2) and (3) are identical and, evidently, there is no longer need to use a four-sublattice model. From the two-magnon scattering experiments, we have shown that the difference between J_{12} and J_{14} is very small, which thus allows us to neglect the effects related to the occurrence of four sublattices. In the above discussion, we have disregarded the fact that, even supposing only one exchange integral, the other anisotropy coefficients can, in principle, give rise to a four-sublattice system, but here again, since the coefficients responsible for such a complication are small, the two-sublattice model is expected to be satisfactory.

Finally, it has to be pointed out that the neglect of the effects related to the existence of four sublattices may not be a good approximation when studying other excitations where the single-ion anisotropy terms play an important role, and where there is no reason to predict *a priori* that the interionic interaction can be described, using a unique next-neighbor exchange coefficient. Such situations, where magnons are well described using a two-sublattice model, and where a correct interpretation of high energy excitons needs a four-sublattice model, occur, in Cr_2O_3 for instance, and have been investigated experimentally as well as theoretically.[20,21]

B. Temperature Dependence of Two-Magnon Raman Scattering

The temperature dependence of the line has been studied. The results are very similar to those previously published concerning two-magnon spectra in other crystals.[13] There is still evidence of scattering above the ordering temperature. Figure 4 shows the variation of the relative frequency at maximum intensity (normalized to 1 at $T=0$ °K). As expected, when the temperature increases, its shift is smaller than for the one-magnon line where it is simply related to the sublattice magnetization (see Sec. VI).

The variation of the normalized frequency versus the normalized temperature T/T_N is exactly the same for $KNiF_3$[13] and for $NaNiF_3$ if one uses T_N = 246 °K for $KNiF_3$, a value derived from recent measurements,[22] and $T_N = 156$ °K for $NaNiF_3$[23] as shown in Fig. 5.

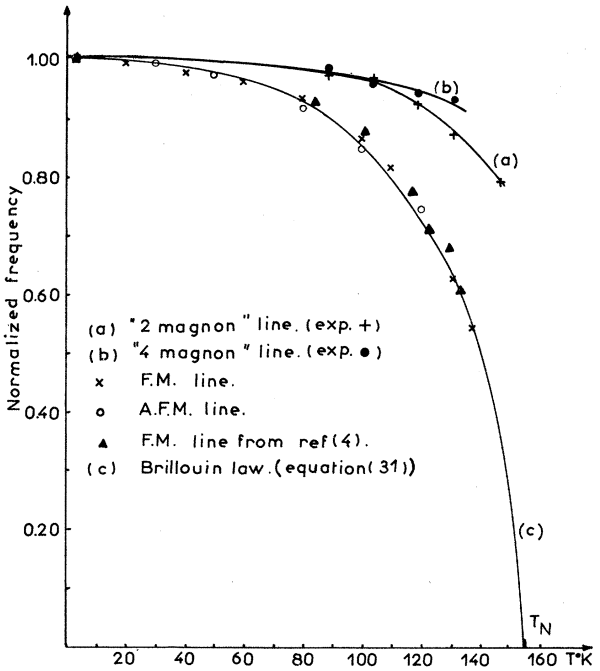

FIG. 4. Variation of the normalized FM, AFM, two-magnon, and (tentatively identified) four-magnon frequencies vs temperature; $H=0$.

The exchange integral value for $KNiF_3$ was found to be 70.5 ± 0.8 cm^{-1}.[13] If we assume that the ratio of the Néel temperatures of $NaNiF_3$ and $KNiF_3$ is equal to the ratio of their exchange integrals we find, for $NaNiF_3$, $T_N = 146$ °K, in very good agreement with measured values (149 °K[1,3] or 156 °K[23]).

C. Comparison of $J\langle S\rangle$ Determination with the Previously Estimated Value

From static magnetic measurements data and antiferromagnetic resonance results, Golovenchitz *et al.*[4] found $J\langle S\rangle = 35$ cm^{-1} at 77 °K. We did not try to calculate the exchange parameters from our $T=77$ °K experiments, since the theory of the temperature dependence of two-magnon Raman scattering is not completely understood. However, the 35-cm^{-1} value is significantly lower than ours; the lowering of the sublattice magnetization is not sufficient to explain the discrepancy since at 77 °K we calculated it, using Ref. 4 data and results, to be equal to $0.93g\mu_B$ (μ_B is the Bohr magneton and g is the effective Lande factor defined in Sec. V). As discussed in Sec. VI, our feeling is that the Golovenchitz *et al.* value is underestimated.

D. Four-Magnon Raman Scattering

Finally, we have investigated four-magnon Raman scattering which has been recently observed in NiO and $KNiF_3$.[24] At 2 °K, there is a broad weak line

centered at 710 cm^{-1}: This frequency is higher than the two-magnon frequency at maximum intensity by a factor 1.6, to be compared with the 1.7 value found for the four-magnon scattering in $KNiF_3$. The temperature dependence study shows an absolute shift towards low frequencies, slightly more marked than for the two-magnon line but the relative shift (Fig. 4) is smaller. However, the line seems to be superimposed to a two-phonon-scattering spectrum and the measurements suffer from a lack of precision. Our identification is only tentative: The large temperature dependence implies that the line is related to magnetic excitations, and its high frequency is not compatible with an magnetic-impurity mode. One cannot completely disregard the possibility of a combined magnon-phonon excitation, although to our knowledge, such a process has never been reported experimentally in a Raman-scattering study. However, in NiO[14,25] and $KNiF_3$,[24] a line involving a two-magnon plus one-phonon emission has been observed by infrared absorption.

V. LOW-FREQUENCY MAGNETIC EXCITATIONS STUDY BY RAMAN SCATTERING

A. Expressions for Equilibrium Positions and Resonance Frequencies

Here we summarize previous theoretical work by various authors[4,27,28] to obtain expressions which are needed for Sec. V B. The results are equivalent to those previously published, but in some cases the notations are slightly different.

For the low-frequency $\vec{k}=\vec{0}$ magnon excitations we need to take into account the various anisotropy terms of the Hamiltonian. If we make the approximation of a two-sublattice weak ferromagnet, according to the symmetry, the equilibrium positions and the resonance frequencies are derived using the following expression of the free energy (which here is normalized in order to refer to one pair of antiferromagnetic neighbors):

$$F=\alpha^2[E\vec{S}_1\cdot\vec{S}_2+\vec{D}\cdot(\vec{S}_1\times\vec{S}_2)+J_{xx}S_{1x}S_{2x}+J_{zz}S_{1z}S_{2z} - A_{xz}(S_{1x}S_{1z}-S_{2x}S_{2z})-A_{xx}(S_{1x}^2+S_{2x}^2)-A_{zz}(S_{1z}^2+S_{2z}^2)] - \alpha\mu_B(\overleftrightarrow{g}_1\vec{S}_1+\overleftrightarrow{g}_2\vec{S}_2)\cdot\vec{H}, \quad (4)$$

where $\vec{S}_1$ and $\vec{S}_2$ are unit vectors (spin 1) and α is the relative magnetization of each sublattice. It has to be identified with the $\langle S\rangle$ coefficient in Sec. IV (it will be taken equal to 1 for $T=0$). x, y, and z stand for components parallel to a, b, and c, respectively. The first term in the development is the isotropic exchange: From the two-magnon Raman scattering it results that the intrasublattice exchange can be ignored, and that the isotropic exchange is well described using only one coefficient J; it follows that $E=Jz$. $\vec{D}\cdot(\vec{S}_1\times\vec{S}_2)$ represents the antisymmetric Dzialoshinski–Moriya interaction, and one shows that $\vec{D}$ is parallel to c. The two following terms come from symmetric anisotropic exchange. The last ones describe the single-ion anisotropy and the effect of an applied magnetic field. The $\overleftrightarrow{g}$ tensor has the following form:

$$\overleftrightarrow{g}_i=\begin{pmatrix} g_{xx} & 0 & \pm g_{xz} \\ 0 & g_{yy} & 0 \\ \pm g_{zx} & 0 & g_{zz} \end{pmatrix} \text{ with } \begin{cases} + \text{ for } i=1 \\ - \text{ for } i=2. \end{cases} \quad (5)$$

Note that α depends upon the temperature but that *a priori* all the temperature dependences may not be described by supposing that the other coefficients remain constant when T changes. However, their temperature variation is expected to be small, at least for the exchange terms where it occurs from the slight changes in distances and angles.

The equilibrium positions are given minimizing F with respect to the $\vec{S}_1$ and $\vec{S}_2$ orientations. One then finds the resonance frequencies, using the equations of motion:

$$\alpha\hbar\dot{\vec{S}}_i=-\vec{S}_i\times\frac{\partial F}{\partial\vec{S}_i}. \quad (6)$$

For $\vec{H}=\vec{0}$, at equilibrium $\vec{S}_1$ and $\vec{S}_2$ are nearly

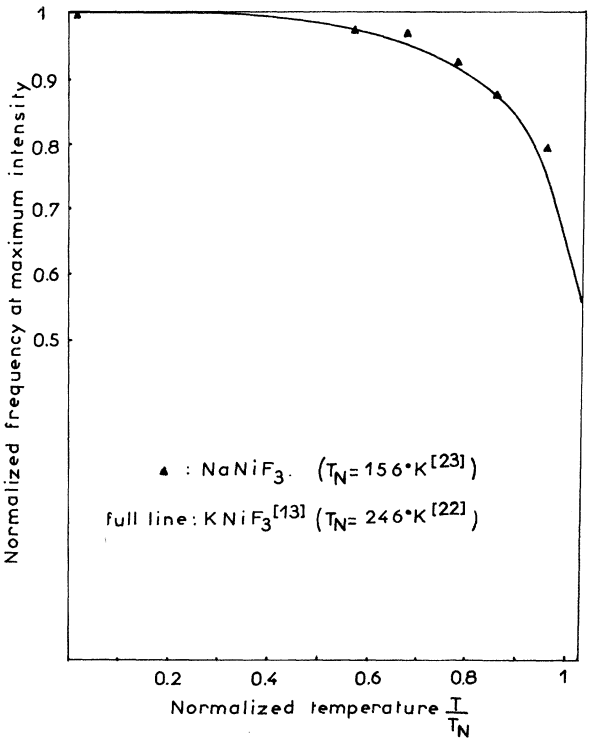

FIG. 5. Comparison of the variation of the normalized two-magnon frequency vs the normalized temperature T/T_N in $NaNiF_3$ (taking $T_N=156$ °K, Ref. 23) and $KNiF_3$ (Ref. 13) (taking $T_N=246$ °K, Ref. 22).

opposite, in the (a, c) plane: They make a small angle $\varphi \simeq (A_{xz}+D)/E$ with c.

Under an applied magnetic field of modulus H along b or c, the two resonance frequencies are given by

$$\left.\begin{aligned} U^2_{xy,c} &= \hbar^2\omega^2_{xy} = U^2_{xy,c} + K_{xy}H + g^2_{zz}\mu_B^2H^2 \\ U^2_{z,c} &= \hbar^2\omega^2_{z,c} = U^2_z + k_z H \end{aligned}\right\} \text{for } \vec{H} \parallel c \qquad (7),\ (8)$$

and

$$\left.\begin{aligned} U^2_{xy,b} &= \hbar^2\omega^2_{xy,b} = U^2_{xy} + L^2_{xy}H^2 \\ U^2_{z,b} &= \hbar^2\omega^2_{z,b} = U^2_z + L^2_z H^2 \end{aligned}\right\} \text{for } \vec{H} \parallel b \qquad (9),\ (10)$$

where

$$U^2_{xy} = [4(E+A'_{xx})(A'_{xx}-A'_{zz}) + 4A_{xz}(A_{xz}+D)]\alpha^2, \qquad (11)$$

$$U^2_z = [4(E+A'_{xx}-A'_{zz})A'_{xx} + (A_{xz}+D)^2]\alpha^2, \qquad (12)$$

$$K_{xy} = \alpha g_{zz}(D+5A_{xz}+2\tau_2 E)\mu_B, \qquad (13)$$

$$K_z = \alpha g_{zz}(D+A_{xz}+2\tau_2 E)\mu_B, \qquad (14)$$

$$L^2_{xy} = g^2_{yy}\frac{A^2_{xz}}{4EA'_{zz}+(D+A_{xz})(D-3A_{xz})}\mu_B^2, \qquad (15)$$

$$L^2_z = g^2_{yy}\frac{4EA'_{zz}(D-A_{xz})^2}{4EA'_{zz}+(D+A_{xz})(D-3A_{xz})}\frac{\mu_B^2}{4}, \qquad (16)$$

with

$$A'_{xx} = A_{xx} + \tfrac{1}{2}J_{xx},$$
$$A'_{zz} = A_{zz} + \tfrac{1}{2}J_{zz}, \qquad (17)$$
$$\tau_1 = g_{xz}/g_{xx}, \quad \tau_2 = g_{zx}/g_{zz}.$$

If $\vec{H}$ is parallel to a, the crystal suffers a spin-flip transition for a critical field H_c. Below H_c, the expressions for the resonance frequencies are rather complex, but above H_c one easily shows that they are obtained in a straightforward way from the formula for $\vec{H} \parallel c$ by permutation of the x and z indices, with a change of sign for the coefficients involving the xz indice. One finds for H_c

$$0 = U^2_{zy} + K_{zy}H_c + g^2_{xx}\mu_B^2H_c^2 \quad (H_c > 0), \qquad (18)$$

and for the resonance frequencies

$$\left.\begin{aligned} U^2_{zy,a} &= \hbar^2\omega^2_{zy,a} \\ &= U^2_{zy} + K_{zy}H + g^2_{xx}\mu_B^2H^2 \\ U^2_{x,a} &= \hbar^2\omega^2_{x,a} = U^2_x + K_x H \end{aligned}\right\} \text{for } \vec{H} \parallel a,\ H > H_c, \qquad (19),\ (20)$$

where

$$U^2_{zy} = -[4(E+A'_{xx})(A'_{xx}-A'_{zz}) - 4A_{xz}(D-A_{xz})]\alpha^2, \qquad (21)$$

$$U^2_x = [4(E+A'_{zz}-A'_{xx})A'_{zz} + (D-A_{xz})^2]\alpha^2, \qquad (22)$$

$$K_{zy} = \alpha g_{xx}(D-5A_{xz}-2\tau_1 E)\mu_B, \qquad (23)$$

$$K_x = \alpha g_{xx}(D-A_{xz}-2\tau_1 E)\mu_B. \qquad (24)$$

B. Experimental Results and Analysis

1. *Observed Spectrum*

At 1.8 °K, we observe two Raman lines centered at 6.5 ± 0.3 cm^{-1} [ferromagnetic (FM) line] and $11.5_5 \pm 0.3$ cm^{-1} [antiferromagnetic (AFM) line]. The FM line strongly scatters only in the α_{xz} and α_{yz} polarizations, whereas the AFM line scatters in α_{xy} polarization. Figure 6 shows a typical spectrum at 2 °K. The intensities are of the same order of magnitude, and smaller than the two-magnon scattering integrated intensity by about a factor of 30. As shown on Fig. 7, the spin-flip transition for $\vec{H} \parallel c$ occurs for $H_c \simeq 20$ kG. In fact, as well known, the sharpness of the transition region is very sensitive to the crystal orientation; consequently, with our experimental arrangement which did not allow a very accurate orientation, the transition region is broad and the FM line frequency does not go down to 0 at $H = H_c$. Figures 8–10 show the frequency shifts versus H for different directions of the magnetic field, in a form convenient for their analysis. We have noted that, for $\vec{H} \neq \vec{0}$, the selection rules are slightly modified. In particular with $\vec{H} \parallel a$ the AFM line also appears in α_{yz} polarization.

The temperature dependence of the frequencies at $\vec{H} = \vec{0}$ is shown on Fig. 4: The relative frequency $U(T)/U(0)$ follows the same law for the FM and the AFM lines. The lines are observed until $T = 137$ °K.

In the range 2–137 °K, the experimental widths at half-maximum remain equal to the instrumental one (1.8 cm^{-1}), which means that the natural width is smaller than 0.5 cm^{-1}. It has been re-

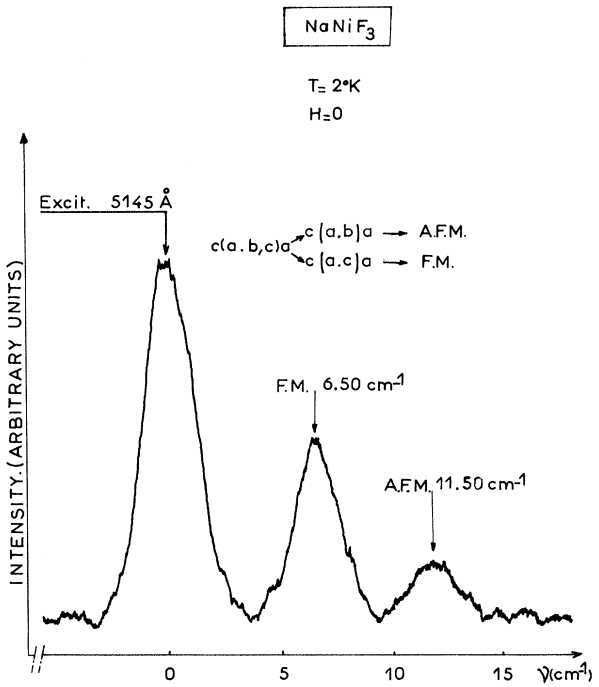

FIG. 6. Typical spectrum showing the FM and AFM lines at $T = 2$ °K. Here the scattered beam is unpolarized, allowing for simultaneous recording of both lines.

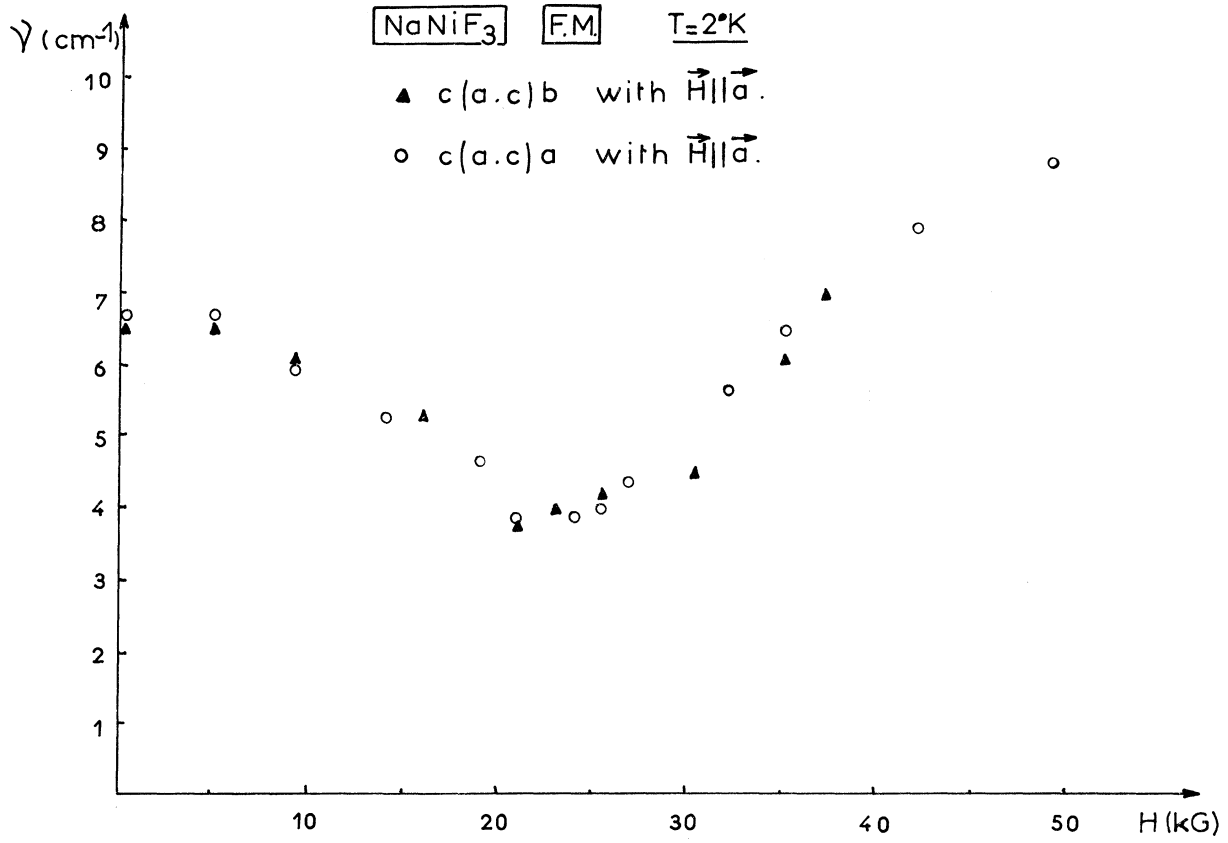

FIG. 7. Variation of the FM line frequency vs H for $\vec{H} \| a$.

cently shown[29] that one of the numerous absorption lines of iodine around 5145 Å, may completely absorb a very sharp Raman line. Since we did not observe very marked changes of intensity when shifting the magnon Raman lines using a magnetic field, we conclude that the iodine absorption lines are not broader than the Raman lines; the widths of the FM and AFM lines are then thought to be at least of the order of 0.05 cm^{-1} even at 2 °K. Although no systematic quantitative analysis of the

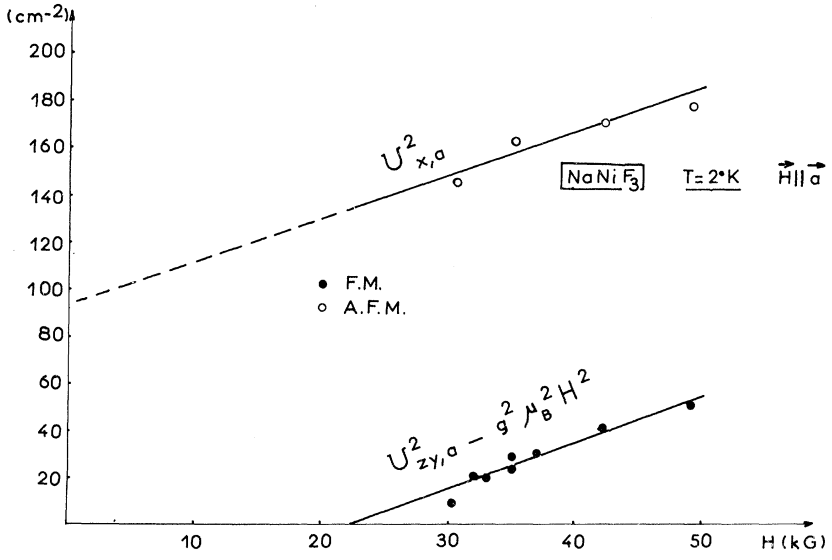

FIG. 8. Graphic analysis of the variation of the FM and AFM lines frequencies for $\vec{H} \| a$.

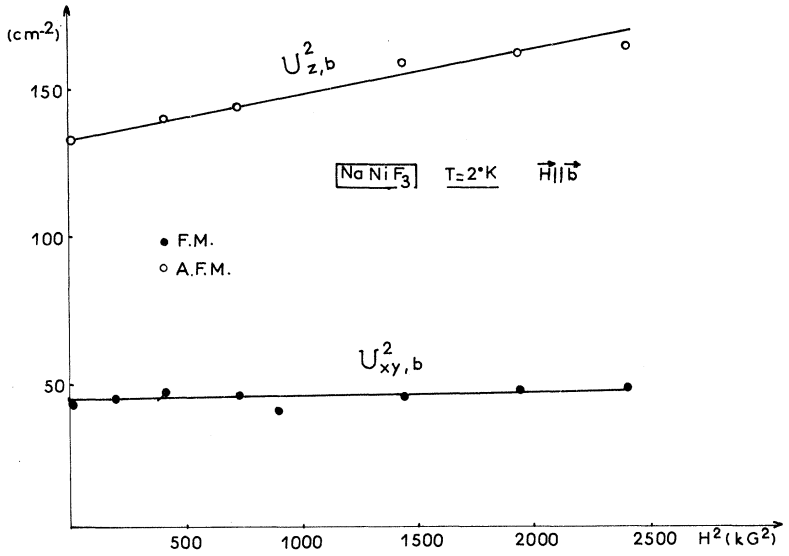

FIG. 9. Graphic analysis of the variation of the FM and AFM lines frequencies for $\vec{H} \| b$.

temperature dependences of the intensities was undertaken, it clearly appears that, for both lines, the intensity significantly increases when increasing temperature until about 100°K; it then begins to decrease above 100 °K. At low temperature this behavior is well understood, considering that the thermal population increase is the dominant effect (note also, as shown on Fig. 11, that the anti-Stokes spectrum, completely absent at 2 °K, is easily observed at 20 °K and above). The high-

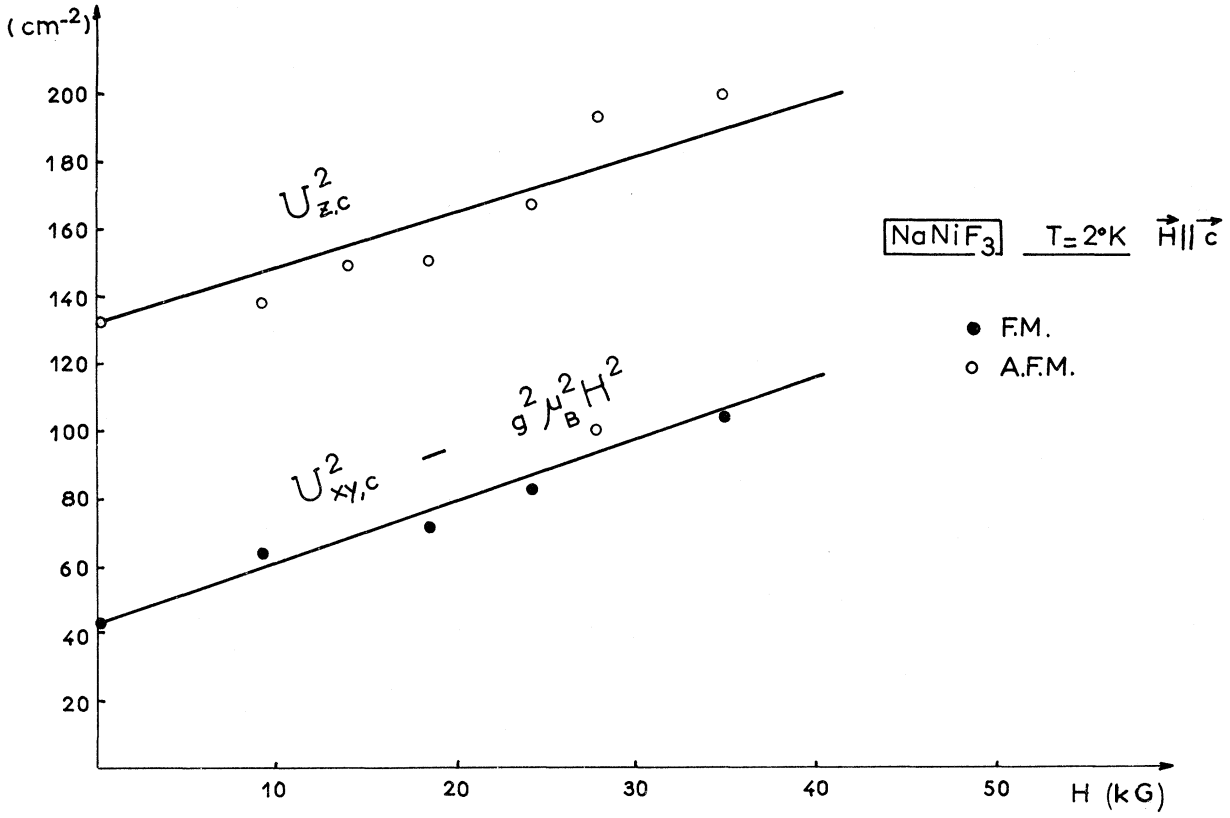

FIG. 10. Graphic analysis of the variation of the FM and AFM lines frequencies for $\vec{H} \| c$.

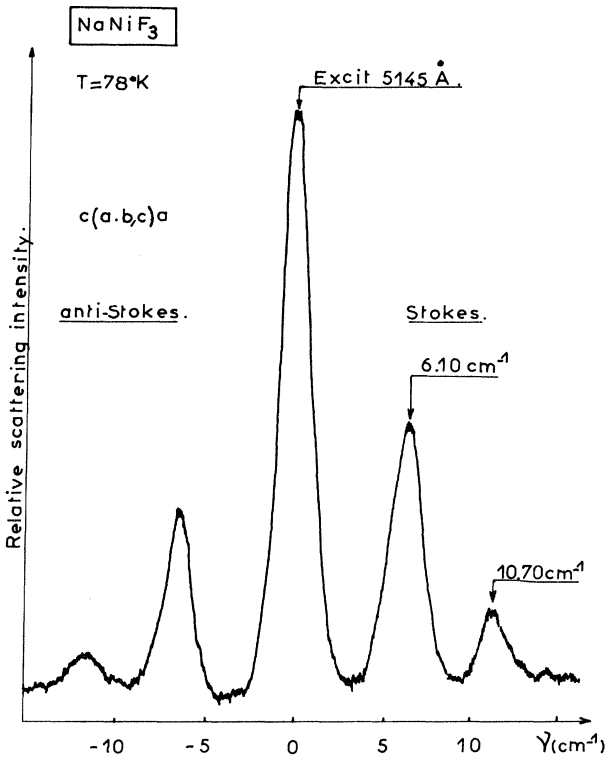

FIG. 11. Typical spectrum showing the FM and AFM lines at $T=78$ °K. Here the scattered beam is unpolarized allowing for simultaneous recording of both lines. Stokes and anti-Stokes spectra are observed.

temperature variation, not due to broadening, disagrees with previous theoretical studies, concerning the case of two-sublattice simple antiferromagnets, which predict a monotonic increase below T_N.[30] However, they agree with experimental results reported in Ref. 30.

2. *Interpretation of Experimental Selection Rules*

At least in zero field the selection rules are in agreement with the theoretical predictions derived using the magnetic point group $D_{2h}(C_{2h})$ where the twofold unitary axis is parallel to c. As pointed out above, at $\vec{k}=\vec{0}$ the two magnon branches, respectively, belong to the Γ_1^+ and to the Γ_2^+ representations of C_{2h} (indeed, supposing four sublattices, there are $2\Gamma_1^+$ and $2\Gamma_2^+$ magnons, but there are two optical Γ_1^+ and Γ_2^+ branches with high frequencies, of about $\sqrt{32}J$). If we now assume that for one-magnon scattering the Raman tensor is antisymmetric, which is normally expected,[11] we predict α_{xy} polarization for Γ_1^+ and α_{xz} and α_{yz} for Γ_2^+.[6,31] Note that NiF_2 is also described by the $D_{2h}(C_{2h})$ magnetic point group and that the published experimental selection rules for magnon scattering in NiF_2[32] are the same as in $NaNiF_3$.

3. *Determination of Coefficients Defining Free Energy*

Although, theoretically, at $T\simeq 0$, most of the coefficients entering into expression (4) could be derived from the experimental results, the limited precision of our data would provide a very imprecise determination of some of them. It is much more efficient to make the following assumptions which are believed to be true within a good approximation.

(i) We use $E=Jz=251$ cm^{-1} and $S=1$, as justified above.

(ii) We suppose a nearly isotropic $\overleftrightarrow{g}$ tensor: The g value differs from 2 because of the spin-orbit coupling between the $^3A_2$ crystalline field state and the $^3T_2$ excited one.[33] The $\overleftrightarrow{g}$ tensor anisotropy arises from the low-symmetry terms of the crystalline field which, to first order, split $^3T_2$ only; as they are expected to be small compared to the $^3A_2$-$^3T_2$ separation Δ, the g anisotropy has to be very small too. The consistency of the assumption will be verified *a posteriori* since we shall find very small single-ion anisotropy terms which have the same origin. Very roughly,

$$\rho\simeq\lambda\delta g, \tag{25}$$

where λ is the spin-orbit coupling constant, ρ and δg being typical values of the single-ion anisotropy coefficient and of the g anisotropy amplitude, respectively.[34] We have, approximately, $g\simeq 2+8\lambda/\Delta$. From spectroscopical data[35] and usual values in other Ni^{2+} compounds,[32,36] we take $g_{xx}=g_{yy}=g_{zz}=g=2,3$, which is probably exact within 1%. However, from the examination of Eqs. (13) and (14), and (23) and (24), it is clear that τ_1 and τ_2, even when small, can play a non-negligible role, since they always appear multiplied by E which is the most important coefficient in (4). A careful examination of the equations shows that it is hopeless to get a precise value of τ_1 and τ_2 separately. Consequently, we assume, following Golovenchitz *et al.*[4] that $\tau_1\simeq\tau_2=\tau$.

Now, using any set of three equations among (13), (14), (23), and (24), we can derive D, A_{xz}, and τ. The three different sets of equations provide three different sets of results: The obtained mean values are $D=16.9\pm1$ cm^{-1}, $A_{xz}=0.1_5\pm0.5$ cm^{-1}, and $E\tau=-0.6\pm1.2$ cm^{-1}. Using those mean values we obtain from (11) and (12) $A'_{xx}=-0.15_5\pm0.03$ cm^{-1} and $A'_{zz}=-0.18_5\pm0.05$ cm^{-1}. Note that there are no means to evaluate separately A_{xx} and J_{xx} or A_{zz} and J_{zz}. Comparing (12) to (22) now provides a new value for A_{xz}: $A_{xz}=0.1$ cm^{-1}, which lies within the uncertainty range of the previous result. We also verify that U_{xy}^2 and U_{zy}^2 are nearly equal, which is consistent with the small value of A_{xz}. At this stage we have not used the variation of the frequencies versus a magnetic field along b

[expressions (15) and (16)]; from Eq. (15), it appears that $U_{xy,b}$ is practically independent of H in agreement with the experiments (Fig. 9); on the other hand, we calculate a theoretical value of L_z equal to 0.107 (cm^{-1}/kG) which is slightly lower, but still in agreement with the 0.12 experimental one. The experimental value of H_c (extrapolated from the FM line frequency variation above H_c for $\vec{H} \parallel a$) is 19.5 kG. The above coefficients lead to $H_c = 11$ kG, but the uncertainty upon A_{xz} easily explains the discrepancy (changing A_{xz} into $-A_{xz}$ gives $H_c = 27$ kG!).

We conclude that our experimental study allows us a consistent determination of the coefficients in expression (4): Unfortunately, owing to the experimental limitations, some of them are known with a rather poor accuracy. The calculated coefficients are listed on the first line of Table II. In view of a comparison with other experiments we have also expressed them in magnetic field units, putting

$$H_E = \frac{\alpha E}{g\mu_B}, \quad H_D = \frac{\alpha D}{g\mu_B}, \quad H_\tau = \frac{\alpha E\tau}{g\mu_B}, \quad H_{A_{xz}} = \frac{\alpha A_{xz}}{g\mu_B}; \tag{26}$$

$$H_{A'_{xx}} = \frac{\alpha A'_{xx}}{g\mu_B}, \quad H_{A'_{zz}} = \frac{\alpha A'_{zz}}{g\mu_B}, \quad H_{A_{x-z}} = \frac{2\alpha(A'_{xx} - A'_{zz})}{g\mu_B}.$$

Finally, that the temperature dependence of the relative FM and AFM frequencies (normalized to 1 at $T = 0$) is the same suggests that all the coefficients, except α, are independent of the temperature; although, in principle, we would need supplemental data concerning the temperature dependence of the spectra with an applied magnetic field, to measure separately the variation of each coefficient. This probable conclusion provides an additional interest to write the free energy using the expression (4).

4. *Absence of Observed Optical Magnon Mode and Validity of Two-Sublattice Model*

We did not find any Raman scattering of magnetic origin around the expected frequencies of the optical $\vec{k} = \vec{0}$ magnons ($\sqrt{32}\,J \simeq 235$ cm^{-1}). Although, in this frequency region the magnon scattering could be hidden by the phonon scattering, the absence of an optical magnon spectrum enforces our assumption that the two-sublattice model provides a very good approximation for the study of magnons in $NaNiF_3$. The four-sublattice model has been studied theoretically.[37] It appears that among the numerous coefficients involved in the four-sublattice model, only relatively few can be determined, but that when the anisotropy energy is small compared to the antisymmetric exchange, which is the case in $NaNiF_3$, it is possible to describe the low-frequency behavior on the basis of a formal two-sublattice model; one has to use effective single-ion anisotropy coefficients which include hidden contributions of an exchange character. In conclusion, even if four-sublattice effects cannot be completely neglected, the above-determined phenomenological coefficients correctly give an account of most of the experimental properties.

VI. DISCUSSION AND COMPARISON WITH PREVIOUS RESULTS

A. Comparison with Antiferromagnetic Resonance Results

Some of the above calculated coefficients had been previously evaluated from antiferromagnetic resonance (AFR) experiments.[4] However the authors could not derive A'_{xx} and A'_{zz}, and for the calculation of the other parameters they needed to take into account the results of magnetic static measurements,[23] using the value of the spontaneous moment σ_{z0} and of the susceptibility χ_c, perpendicular to the sublattice magnetization, which have to equal

$$\sigma_{z0} = g\mu_B\alpha\,[(D + A_{xz} + 2E\tau)/E](2/v), \tag{27}$$

$$\chi_c = (g^2\mu_B^2/E)(2/v), \tag{28}$$

where v is the volume of the orthorhombic unit cell.

The main advantage of the present study is the possibility of a calculation of the anisotropy and exchange coefficients which is completely independent of other measurements (except for the evaluation of g). Note also that we get results at 2 °K which normally provide an easier physical interpre-

TABLE II. Coefficients describing the magnetic properties of $NaNiF_3$. First line, calculation from our data at 2 °K; second line, calculation from our measurements at 2 °K supposing that only α is temperature dependent; third line, comparison with antiferromagnetic resonance data from Ref. 4 and using Eq. (31).

T (°K)	α	g	E (cm^{-1})	H_E (kG)	τ	$E\tau$ (cm^{-1})	H_τ (kG)	D (cm^{-1})	H_D (kG)	A_{xz} (cm^{-1})	H_{xz} (kG)	A'_{xx} (cm^{-1})	H'_{xx} (kG)	A'_{zz} (cm^{-1})	H'_{zz} (kG)	H_{x-z} (kG)
2	1	2.30	251	2350	0.0025	−0.6	−6	16.9	157	$+0.1_5$	+1.5	-0.15_5	-1.4_5	−0.19	-1.7_5	$+0.6$
77[a]	0.93	2.30	251	2180	0.0025	−0.6	−6	16.9	146	$+0.1_5$	+1.5	-0.15_5	-1.3_5	−0.19	−1.6	$+0.5$
77[b]	0.93	2.14	226	2100	0.0120	−2.7	−25	17.4	162	+1.3	+12	n.m.[c]	n.m.	n.m.	n.m.	−1.1

[a]Calculated from our measurements at 2 °K supposing that only α is temperature dependent.

[b]From Ref. 4, and using Eq. (31).

[c]Not measured.

tation. On the other hand, unfortunately, the experimental accuracy of frequency measurements is of the order of 0.3 cm^{-1}, which gives a relatively low precision at low frequencies. However, the experimental determination of E is very accurate. We think that the values of D, A'_{xx}, and A'_{zz} are correct within less than 10%. In contrast, the relative uncertainty concerning A_{xz} and $E\tau$ is high, the absolute accuracy being around 0.5 cm^{-1}. On the second line of Table II we give the calculated values of the coefficients at 77 °K, using the temperature dependence of the measured frequencies, and supposing that only α varies with the temperature: One finds $\alpha = 0.93$ at $T = 77$ °K. We have also calculated α, from published data of Golovenchitz *et al.*,[4] with the help of expression (28), which they claim to have used for their analysis. Here again we find $\alpha = 0.93$, which confirms that the frequencies are simply proportional to the sublattice magnetization, and also indicates that at $T \simeq 0$ °K the zero point sublattice demagnetization is very small. On the third line of Table II we have reported the coefficients derived from Ref. 4. When comparing lines 2 and 3 we see that the agreement for H_E and D is very good, while it is poorer for E and H_D. It is not clear to us how the results were derived in Ref. 4, since, apparently only six independent equations were used to calculate seven independent coefficients, namely, Eqs. (11)–(14), (27), and (28) to derive g, τ, α, H_E, H_τ, H_{xz}, H_{x-z} [the quadratic term of the field dependence of frequencies in expressions (7) and (19) provides then only a very crude estimate of g]. However in our opinion the 2.14 g value used in Ref. 4 is certainly underestimated, when compared to theoretical predictions and experimental results in other similar Ni salts. We then think that our determination of E is the most precise; it can be objected that we have completely neglected the intrasublattice isotropic exchange (next-nearest-neighbor exchange) which would make E differ from half the cutoff frequency of the two-magnon Raman scattering line, but as pointed out previously, if not very small, such an exchange would make the two-magnon Raman scattering line shape differ from the theoretical one, calculated by neglecting the occurrence of four sublattices, the anisotropy terms and the next-nearest-neighbors exchange.

In our opinion, the divergences concerning the other coefficients cannot be explained only from experimental uncertainties; it would be of interest to know if another choice of g could provide different values from the analysis of AFR spectra. In any case, all the anisotropy coefficients except D, are small compared to E. Although they play a substantial role in the expression of the FM and AFM frequencies, they are completely negligible for high frequencies excitations.

B. Orders of Magnitude of D and J_{xx} (J_{zz})

A very crude estimate of the orders of magnitude of D and J_{xx} (or J_{zz}) leads to[38]

$$D \sim [(g-2)/g]E \sim (\lambda/\Delta)E, \tag{29}$$

$$J_{xx}(J_{zz}) \sim [(g-2)/g]^2 E \sim (\lambda^2/\Delta^2)E. \tag{30}$$

D is expected to be one order of magnitude smaller than E, and $J_{xx}(J_{zz})$ to be one order of magnitude smaller than D. The experimental results then agree with values predicted by (29) and (30).

From the rough estimate of the single-ion anisotropy terms [expression (25)] we expect them to be of the order of $\lambda\tau \simeq 1$ cm^{-1}, which is in agreement with our results.

C. Magnetic Susceptibility and Spontaneous Magnetic Moments

Using expression (27) we have calculated the spontaneous magnetic moment: We find $0.074\mu_B$ per Ni ion at 0 °K and $0.068\mu_B$ at 77 °K. This last value has to be compared to the $0.059\mu_B$ experimental one, resulting from static measurements.[23] The agreement is fair. Moreover, expression (28) allows us to calculate χ_c. We find $\chi_c = 79\times10^{-6}$ in excellent agreement with the experimental value $\chi_c = 77\times10^{-6}$.[23]

D. Sublattice Magnetization

Finally, in the molecular field approximation, the relative magnetization $\alpha(T)$ varies as

$$\alpha(T) = B_S\left(\frac{2S+1}{S}\,\frac{T}{T_N}\right), \tag{31}$$

where $S = 1$ and B_S is the Brillouin function for $S = 1$. As shown in Fig. 4, the normalized frequency exactly follows the above law if we take the previously measured value $T_N = 156$ °K[23]; the fit is less accurate with $T_N = 149$ °K, although in $NaNiF_3$ the sublattice moment has been reported from neutron scattering measurements to follow a Brillouin law with $T_N = 149$ °K.[3]

As pointed out above, the 156 and 246 °K respective ordering temperatures for $NaNiF_3$ and $KNiF_3$ lead to identical variation of the two-magnon normalized frequency versus the normalized temperature T/T_N for the two crystals; if one takes $T_N = 149$ °K, here again the fit is less accurate. A situation where different determinations lead to different Néel temperatures has also been observed in $KNiF_3$.[22,39,40]

The ordering temperature seems sample dependent and very sensitive to defects and impurities. In any case, the fact that the normalized frequencies follow a simple Brillouin law as well as the sublattice magnetization confirms that, except α, the coefficients entering into expression (4) can be

regarded as temperature independent, and justifies the way we have compared our results to antiferromagnetic resonance spectra at 77 °K.

ACKNOWLEDGMENTS

It is a pleasure to thank P. P. Syrnikov, who grew the $NaNiF_3$ crystals.

*Present address: Laboratory of Magnetism, A. F. Ioffe Physico-Technical Institute of the Academy of Sciences of the U.S.S.R., Leningrad K21, U.S.S.R.

[1]S. Ogawa, J. Phys. Soc. Jap. **15**, 2361 (1969).
[2]W. Rudorff, J. Kandler, and D. Babel, Z. Anorg. Allg. Chem. **317**, 261 (1962).
[3]A. Epstein, J. Makovski, M. Melamud, and H. Shaked, Phys. Rev. **174**, 560 (1968).
[4]E. I. Golovenchitz, V. A. Sanina, and A. G. Gurevich, Fiz. Tverd. Tela **11**, 642 (1969) [Sov. Phys.-Solid State **11**, 516 (1969)].
[5]We use the notations of F. Koster, J. O. Dimmock, R. G. Wheeler, and H. Statz, *Properties of the Thirty-Two Point Groups* (MIT, Cambridge, Mass., 1963).
[6]L. N. Ovander, Opt. Spectrosc. **9**, 302 (1960).
[7]M. Balkanski, P. Moch, and M. K. Teng, J. Chem. Phys. **46**, 1621 (1967).
[8]C. H. Perry and E. F. Young, J. Appl. Phys. **38**, 4616 (1967).
[9]I. Nakagawa, A. Tsuchida, and T. Shimanouchi, J. Chem. Phys. **47**, 982 (1967).
[10]A. Okasaki, H. Iwanaga, and N. Tsukida, J. Phys. Soc. Jap. **24**, 209 (1968).
[11]P. A. Fleury and R. Loudon, Phys. Rev. **166**, 514 (1968).
[12]R. J. Elliott, M. F. Thorpe, G. Imbush, R. Loudon, and J. B. Parkinson, Phys. Rev. Lett. **21**, 147 (1968).
[13]S. R. Chinn, H. J. Zeiger and J. R. O'Connor, Phys. Rev. B **3**, 1709 (1971).
[14]R. E. Dietz, G. I. Parisot, and A. E. Meixner, Phys. Rev. B **4**, 2302 (1971).
[15]P. A. Fleury, Phys. Rev. Lett. **21**, 151 (1968).
[16]T. Moriya, in *Magnetism*, edited by G. T. Rado and H. Suhl (Academic, New York, 1963), Vol. I, p. 85.
[17]J. P. Van der Ziel and L. G. Van Uitert, Phys. Rev. **179**, 343 (1969).
[18]It can be shown that for the $D_{2h}(C_{2h})$ group, the symmetry properties are sufficiently specified by the use of the representations of C_{2h}. See J. O. Dimmock and R. G. Wheeler, J. Phys. Chem. Solids **23**, 729 (1962).
[19]R. Loudon, Adv. Phys. **17**, 243 (1968).
[20]J. W. Allen, R. M. MacFarlane, and R. L. White, Phys. Rev. **179**, 523 (1969).
[21]J. W. Allen, Phys. Rev. Lett. **25**, 934 (1970).
[22]J. Nouet, A. Zarembovitch, R. V. Pisarev, J. Ferre, and M. Lecomte, Appl. Phys. Lett. **21**, 161 (1972).
[23]V. M. Judin and A. B. Sherman, Phys. Status Solidi **20**, 759 (1967).
[24]R. E. Dietz, W. F. Brinckman, and A. E. Meixner, Phys. Rev. Lett. **27**, 814 (1971).
[25]R. Newman and R. M. Chrenko, Phys. Rev. **114**, 1507 (1959).
[26]A. Tsuchida, J. Phys. Soc. Jap. **21**, 2497 (1966).
[27]G. F. Hermann, J. Phys. Chem. Solids **24**, 597 (1963).
[28]E. A. Turov, in *Physical Properties of Magnetically Ordered Crystals* (Academic, New York, 1965).
[29]E. Amzallag, C. Dugautier, P. Moch, and M. Balkanski, Solid State Commun. (to be published).
[30]R. Loudon, J. Phys. C **3**, 872 (1970).
[31]A. P. Cracknell, J. Phys. C **2**, 500 (1969).
[32]P. A. Fleury, in *Proceedings of the International Conference of Light Scattering in Solids,* edited by M. Balkanski (Flammarion, Paris, 1972), p. 157.
[33]J. S. Griffith *The Theory of Transistion Metal Ions* (Cambridge U.P., London, England, 1961), p. 347.
[34]T. Moriya, Phys. Rev. **117**, 635 (1960).
[35]R. V. Pisarev, Fiz. Tverd. Tela **7**, 1382 (1965) [Sov. Phys.-Solid State **7**, 1114 (1965)].
[36]M. Peter and J. B. Mock, Phys. Rev. **118**, 137 (1960).
[37]G. F. Hermann, Phys. Rev. **133**, A1334 (1964).
[38]T. Moriya, Phys. Rev. **120**, 91 (1960).
[39]K. Hirikawa and T. Hashimoto, J. Phys. Soc. Jap. **15**, 2063 (1960).
[40]M. E. Lines, Phys. Rev. **164**, 736 (1967).

PHYSICAL REVIEW B VOLUME 7, NUMBER 9 1 MAY 1973

Magnetic Susceptibility of MnF_2 near T_N and Fisher's Relation

E. E. Bragg and M. S. Seehra
Physics Department, West Virginia University, Morgantown, West Virginia 26506
(Received 7 December 1972)

Measurements of the parallel magnetic susceptibility χ of MnF_2 are reported for $60 < T < 80$ °K in temperature intervals of about 0.1 °K. A check on Fisher's relation, viz., $C_m \simeq A\,\partial(\chi T)/\partial T$, is made near the Néel temperature T_N using Teaney's measurements of the magnetic specific heat C_m. General features of Fisher's relation are found to be valid, except A is found to have considerable temperature dependence in the temperature range $|(T - T_N)/T_N| < 0.03$. It is shown that for $T > T_N$ the observed temperature dependence of A can in part be explained by including the effect of the uniaxial anisotropy on the temperature dependence of the transverse correlation functions.

I. INTRODUCTION

It has been shown by Fisher[1] that in a simple antiferromagnet with predominantly short-range interactions, the magnetic specific heat C_m is related to the parallel static susceptibility χ by the relation